CRYSTAL GROWTH & DESIGN

pubs.acs.org/crystal

Article

Assembly of the Intraskeletal Coral Organic Matrix during Calcium Carbonate Formation

Silvia Milita,* Tal Zaquin, Simona Fermani, Devis Montroni, Iddo Pinkas, Luisa Barba, Giuseppe Falini,* and Tali Mass*

Cite This: *Cryst. Growth Des.* 2023, 23, 5801−5811

Read Online

ACCESS | Metrics & More | Article Recommendations | Supporting Information

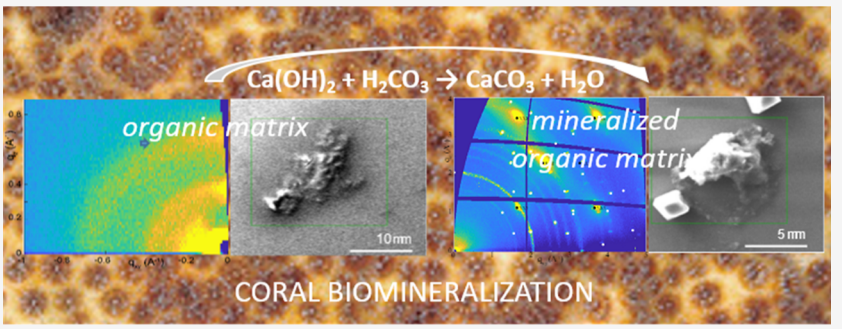

ABSTRACT: Scleractinia coral skeleton formation occurs by a heterogeneous process of nucleation and growth of aragonite in which intraskeletal soluble organic matrix molecules, usually referred to as SOM, play a key role. Several studies have demonstrated that they influence the shape and polymorphic precipitation of calcium carbonate. However, the structural aspects that occur during the growth of aragonite have received less attention. In this research, we study the deposition of calcium carbonate on a model substrate, silicon, in the presence of SOM extracted from the skeleton of two coral species representative of different living habitats and colonization strategies, which we previously characterized. The study is performed mainly by grazing incidence X-ray diffraction with the support of Raman spectroscopy and electron and optical microscopies. The results show that SOM macromolecules once adsorbed on the substrate self-assembled in a layered structure and induced the oriented growth of calcite, inhibiting the formation of vaterite. Differently, when SOM macromolecules were dispersed in solution, they induced the deposition of amorphous calcium carbonate (ACC), still preserving a layered structure. The entity of these effects was species-dependent, in agreement with previous studies. In conclusion, we observed that in the setup required by the experimental procedure, the SOM from corals appears to present a 2D lamellar structure. This structure is preserved when the SOM interacts with ACC but is lost when the interaction occurs with calcite. This knowledge not only is completely new for coral biomineralization but also has strong relevance in the study of biomineralization on other organisms.

INTRODUCTION

Many biomineralization processes occur on a structured substrate which can be a crystalline plane or an array of macromolecules.[1,2] Thus, the growth of a biomineral, the composite inorganic−organic material produced by organisms, is generally a heterogeneous process. A widely studied biomineral is calcium carbonate, which is the main mineral phase associated with invertebrates.[1] In this context, examples of calcium carbonate biominerals are coral skeletons,[3−5] mollusk shells,[6,7] foraminifera shells,[8] coralline red algae,[9] echinoderm endoskeleton, and teeth.[10,11]

Recent studies indicated that in many cases, the growth of biogenic calcium carbonate occurs through the initial formation of amorphous calcium carbonate (ACC) particles that crystallize once anchored to a substrate.[12−14] A series of molecular dynamic simulations showed that the ions on the surface of ACC particles have a higher mobility than their bulk counterparts.[15] This mobility allows them to preferentially interact with acidic amino acids, suggesting that crystallization occurs in this region via solid-state transformation.[16,17] This discovery was experimentally confirmed by applying a combination of high-resolution imaging and in situ solid-state nuclear magnetic resonance spectroscopy.[15] Accordingly with these experiments, the classic theory of crystal nucleation and growth does not apply to biominerals.[18] An important consequence is that one of the experimental proved

Received: April 1, 2023
Revised: July 1, 2023
Published: July 15, 2023

https://doi.org/10.1021/acs.cgd.3c00401
Cryst. Growth Des. 2023, 23, 5801−5811

biomineralization paradigms, i.e., the epitaxial growth of a mineral phase on a macromolecular template,[19−23] seems to need a deeper investigation. Furthermore, the interaction between the ACC particles and the heterogeneous substrate at the atomic and molecular levels has been poorly investigated.

Grazing incidence X-ray diffraction (GIXD) is a technique extensively employed in the study of surfaces of inorganic single crystals, crystal nucleation, and thin films (monolayers and few layers thick) deposited on a flat surface. In GI, the scattered intensities are recorded when the X-ray beam impinges on the surface with a very small incident angles, α_i, close to the critical angle for the total external reflection α_c. As such, the proper choice of the α_i, allows one a depth resolved investigation of the structural properties, due to the dependence of the X-ray penetration depth on the α_i. When $\alpha_i < \alpha_c$ only the surface layers (few Å thick) are probed, while for $\alpha_i > \alpha_c$ several micrometers are investigated. In GI geometry, both the signals scattered at wide (GIWAXS) and small angles (GISAXS) can be recorded, in the GIWAXS or GISAXS techniques, respectively, providing information on periodicities in the order of Å and nm. Diffraction patterns, recorded at wide angles, can be obtained from crystalline structures on surfaces,[24] and in particular, they allow Dutta and co-workers to demonstrate a 1:1 match between the arachidyl sulfate monolayer unit cell and the unit cell of the (001) plane of calcite.[25] This showed that the GIWAXS techniques can be efficiently applied for the study of calcite growth along preferential orientations.

In situ GISAXS was used to measure the nucleation rates at different supersaturations of $CaCO_3$, further providing thermodynamic parameters for subsurface reactive transport modeling regarding $CaCO_3$ formation on surfaces.[26] Plaster samples biotreated were analyzed by microprobe X and GIXD. The results showed only the presence of calcite, no transitory state was observed.[27] X-ray reflectivity (XRR) is a complementary surface technique that produces electron density profiles as a function of distance to the interface and can also provide information on nondiffracting materials.[24] DiMasi and co-workers used XRR to distinguish between the different kinetic effects of polymer, magnesium ions, and mineral ions concentrations on the formation and stabilization of ACC under a fatty acid monolayer.[28] The combination of GIXD and XRR measurements for the study of $CaCO_3$ provides information about the structure of the substrate molecules and crystals formed. This showed that the conformational plasticity of the surface molecules leads to the nucleation of calcite with growth along different crystallographic orientations.[29]

It is reported in literature that the coral biomineralization process occurs by the heterogeneous formation of aragonite fibers on Mg-calcite on which intraskeletal organic molecules are adsorbed.[30,31] Recent studies characterized the soluble fraction (SOM) composition and structure of the intraskeletal organic molecules extracted from different coral species, *Stylophora pistillata* and *Oculina patagonica*.[32] These studies showed that the SOM induced the overgrowth of calcium carbonate on Mg-calcite with different textures in the absence of Mg ions.[33] Here, we further aim to test the role of coral SOM in calcium carbonate deposition. We hypothesize that the presence of SOM adsorbed on a substrate modifies the deposition of calcium carbonate at the molecule−mineral interface, and we aim to study this process by GIWAXS, optical microscopy, scanning electron microscopy (SEM), energy-dispersive X-ray spectroscopy (EDX) mapping, and micro-Raman spectroscopy. To properly perform the experiment, we chose a silicon wafer as substrate on which to adsorb the SOM. The chemical inertness and high flatness of this material is required to accurately control α_i. This substrate does not have relevance in coral biomineralization, where is well-known that mineral deposition starts on the surface of coralline algae and continues on magnesium calcite and aragonite.[34] However, it is the best one to show the potentiality of the GIWAXS techniques, which poses the constraints reported above. The deposition of calcium carbonate was induced using a calcium hydroxide solution and a carbonic acid solution, avoiding the formation of salt coproducts. The SOMs extracted from the skeletons of *S. pistillata* and *O. patagonica* were used. We proposed to study the fast-growing tropical coral *S. pistillata* and the slow-growing temperate coral *O. patagonica*. Those corals represent different growth strategies and diverse growth conditions and, in addition, in a recent study we characterized the SOM of both species.[32]

EXPERIMENTAL SECTION

Preparation of $CaCO_3$ Dispersion. Calcium carbonate was synthesized by mixing equal volumes (300 μL) of both calcium hydroxide and carbonic acid solutions. The latter solution was prepared by bubbling a high-grade carbon dioxide gas into water until a constant pH (3.99) was achieved. The concentration of this solution was then determined by titration using a standard NaOH solution (c = 0.10 M). Calcium hydroxide solution was prepared by adding an excess of calcium hydroxide to water. The suspension was stirred for 3 h and then filtered through a 0.22 μm membrane filter, both processes occurred under an atmosphere of nitrogen. The concentration was determined by titration using the standard HCl solution (c = 0.10 M). In all the experiments, Milli-Q water (conductivity <0.1 mS cm^{-1}) was used. The freshly prepared carbonic acid solution, pure or with the required amount of dissolved SOM was always poured into the calcium hydroxide solution.

SOM Extraction. Approximately 2.5 g of powdered skeleton was treated overnight with 200 mL of sodium hypochlorite (5 vol %) solution. Successively the powder was washed with water and lyophilized. The surface cleaned skeleton powder was used from each sample to extract the coral skeletal soluble organic macromolecules (SOM) using the method described in Reggi et al. (2020).[35] In brief, powdered samples were poured into a dialysis bag (MWCO 3500 Da) with a small volume of water. The dialysis bag was immersed in a 0.1 M acetic acid solution until complete dissolution of the mineral phase. Samples were then centrifuged at 5000g for 5 min at 4 °C, and the supernatant was collected and lyophilized. The SOM concentration (μg/mL) was expressed as the amount of protein from the amino acid analysis.

Silicon Wafer Substrate Preparation. SiO_2/Si substrates 1 × 1 cm^2 were sequentially sonicated in DI water, acetone, and isopropyl alcohol for 10 min each.

Deposition of SOM $CaCO_3$ and $CaCO_3$/SOM Mix on Silicon Wafer Substrates. Freshly prepared 300 μL of the $CaCO_3$ suspension was kept in a plastic vial for a time ranged between 0 and 15 min (t_{mix}). After this period, 100 μL of the suspension was transferred onto the surface of the substrate and left there for a t_{cast} time ranging between 0 and 10:00 min. Finally, the dispersion was spin-coated at 2000 rpm for 2:00 min. These experimental conditions are summarized in Table S1.

Optical Microscopy Observations. Optical microscopy images were collected in the reflection mode using a Leica DM4000 optical microscope. The images were also collected by using crossed-polarizers to check for the presence of birefringence.

SEM Analyses. The SEM images were collected on samples without any coating by using a ZEISS Evo LS10 under low pressure

https://doi.org/10.1021/acs.cgd.3c00401
Cryst. Growth Des. 2023, 23, 5801−5811

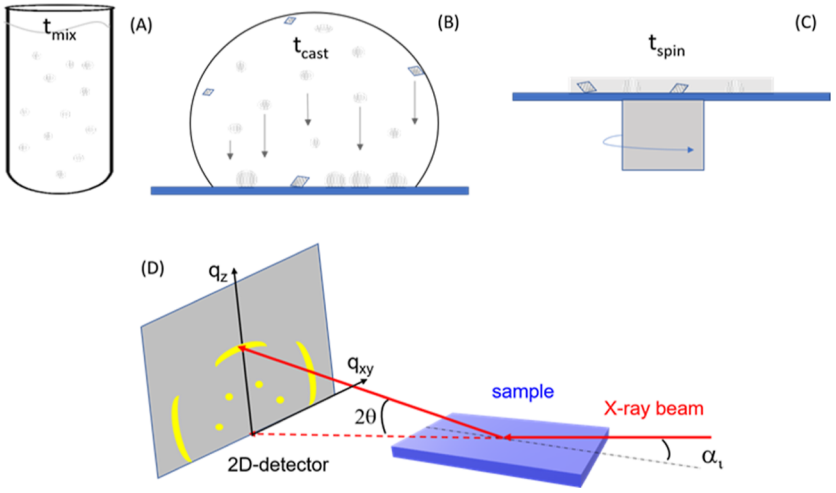

Figure 1. Sequential different stages of sample preparation. (A) Mixing of the reactants, calcium hydroxide, and carbonic acid; t_{mix} indicates the time of mixing. (B) Deposition of the $CaCO_3$ particles on the substrate for a time t_{cast}. (C) Spin coating process to leave a thin layer on the surface. The circles indicate ACC particles and prenucleation clusters, while the rhombuses indicate $CaCO_3$ crystalline particles. (D) Sketch of the GIWAXS setup. The dots and arcs on the 2D detector represent diffraction signals from highly and weakly oriented crystallites, respectively.

operating at 30 kV. EDS spectra and maps were recorded using an X-rays EDS spectrometer Bruker Quantax 200 × 30 mm^2.

Micro-Raman Spectroscopy Measurements. Raman measurements were conducted on a LabRAM HR Evolution instrument (Horiba. France). The instrument is equipped with an 800 mm spectrograph which allows for sub-two wavenumber pixel spacing when working with 1800 grooves/mm grating at 325 nm excitation. The sample was exposed to the laser light by an ×40 Near UV NA = 0.47 objective (LMU-40×-NUV, Thorlabs. USA). The LabRAM instrument has a 1024 × 256 pixel open-electrode, front-illuminated, and cooled CCD camera. The system is set around an open confocal microscope (BX-FM Olympus. Japan) with a spatial resolution better than 2 μm by using the 40× Near UV objective. Exposure was set according to the signal intensity, which required exposure between 15 s and 1 min. This system is equipped with ultralow frequency capability, four laser lines, many objectives, and several gratings to allow modular and flexible use for samples of significant variability.

Grazing Incidence Diffraction Measurements. GIWAXS measurements were performed at the XRD1 beamline of the ELETTRA, a synchrotron radiation facility in Trieste, Italy. A Pilatus X-ray detector (DECTRIS Ltd. Baden, Switzerland) was used to collect the 2D images. The sample detector distance was 200 mm. The wavelength was fixed to λ = 0.7 Å and the beam size was of 200 × 200 μm^2. Different X-ray beam incident angles α_i were selected, below and above the critical angle for the total reflection (0.07°), to probe the surface layer (few nm) and full film thickness (the X-ray penetration depths are ∼1000 nm).

RESULTS AND DISCUSSION

Experimental Setup. In this research, a crucial initial step was the definition of the experimental setup. The choices were made having in mind the following requests: (i) the formation of prenucleation cluster or crystalline phase precursors should occur in solution; (ii) the mineral phase should preferentially form on the substrate; and (iii) only the formation of a calcium carbonate mineral should take place. To achieve these goals, as the first choice, we precipitated $CaCO_3$ by mixing a solution of calcium hydroxide with a solution of carbonic acid.[36] This $CaCO_3$ precipitation method has been already used in in vitro studies of biomineralization processes where SOM, peptides and several ions have been used as additives.[36−38] When equal volumes (300 μL) of 1.2 × 10^{-2} M H_2CO_3 solution and 1.0 × 10^{-2} M $Ca(OH)_2$ solution were mixed, a milky dispersion appeared. The used concentrations are not related to the concentration of Ca and carbonate ions in seawater. They were mainly selected by the experimental set-up and by the requirement to be above the saturation limit of ACC.[39] This was because several reports indicate that the biomineralization of corals occurs through a transient ACC phase.[40] The initial supersaturation is defined as relative supersaturation, $S - 1$, $S = (\prod/K_{sp})^{1/2}$, where $\prod$ is the ion activity product $a(Ca^{2+})\cdot a(CO_3^{2-})$, and K_{sp} is the thermodynamic equilibrium constant of dissolution of the most stable calcium carbonate polymorph, calcite (K_{sp} = 3.3 × 10^{-9} at 25 °C). From the known total concentrations of $Ca(OH)_2$ and H_2CO_3 initially mixed, the molar concentrations and the corresponding activities of all relevant ionic species that were assumed to exist at considerable concentrations in the solution (H^+, OH^-, CO_3^{2-}, HCO_3^-, $CaCO_3^0$, $CaHCO_3^+$, Ca^{2+}, and $CaOH^+$) were calculated. The detailed calculation procedure, which takes into account the respective proteolytic equilibria and equilibrium constants as well as the charge- and mass-balance equations, has been described previously.[41] The used concentrations allowed to have a mixture with an initial $CaCO_3$ supersaturation with respect to calcite of 22.2 (pH = 9.8) and most importantly, highly supersaturated with respect to all the crystalline polymorphs of $CaCO_3$ and ACC, hence allowing their formation by a spontaneous precipitation process.[39] In this condition of high supersaturation, the deposition of $CaCO_3$ is governed by kinetic processes, which can be defined by the following experimental parameters: the time of mixing (t_{mix}), the time of casting (t_{cast}), and the time of spinning (t_{spin}). t_{mix} represents the period of time that spams from the mixing of the reactants (i.e., calcium hydroxide and carbonic acid solutions) to the deposition on the substrate of a volume (100 μL) of the $CaCO_3$ dispersion. During this time, due to the high starting supersaturation, prenucleation clusters form, some crystalline nuclei may form as well.[42] The deposited volume of $CaCO_3$ dispersion, when observed under an optical microscope with crossed-polarizers (Figure S1), does not show any birefringence for a time shorter than 2 min. Thus, most of the milky material is $CaCO_3$ and has no optical microscope detectable crystalline state. t_{cast} represents the time in which a volume of the $CaCO_3$ dispersion is kept on

https://doi.org/10.1021/acs.cgd.3c00401
Cryst. Growth Des. 2023, 23, 5801−5811

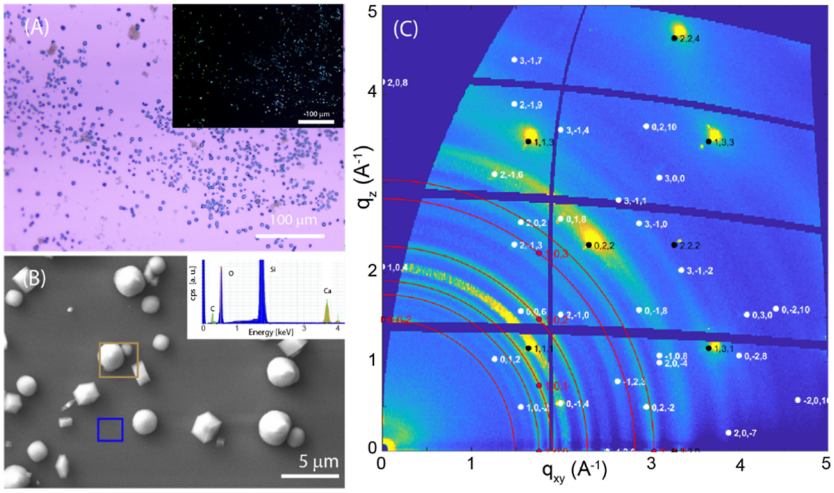

Figure 2. Control experiment on formation of $CaCO_3$ on the surface of a silicon wafer without SOM added. (A) Optical microscopy image and (inset) crossed-polarizer optical microscopy image. (B) SEM image of the sample. The inset reports the EDX spectra of the regions inside the squares according to the colors. (D) 2D-GIWAX image in which the red Debye rings indicate the diffraction effects from vaterite, the white spots are the Bragg peaks from calcite and those black from the silicon substrate. All the diffraction peaks come from vaterite, calcite, and silicon substrate and were indexed according to crystalline structure.[43]

the substrate. During this time, some prenucleation clusters and crystal nuclei continue to form, and eventually small crystals deposit on the substrate, on which nucleation and growth can also occur. t_{spin} is the spinning time, during this process part of the solution is expelled from the substrate, the solvent completely evaporates and a layer of calcium carbonate forms on the substrate. This layer also contains the $CaCO_3$ particles that formed during the casting time. The volume of dispersion that is expelled by the substrate during the spinning process is not quantifiable, but it is reasonable to suppose that it represents most of the volume casted on the substrate. Aiming to have on the substrate mostly the deposition of ACC before the spinning process, and in a quantity high enough to be detected by GIWAXS, a series of optimization experiments was performed (Table S1). A volume of $CaCO_3$ dispersion of 100 μL, a t_{mix} of 1:00 min, and a t_{cast} of 2:30 min were used. A t_{spin} of 2:00 min allowed for a dry precipitate on the substrate a dry precipitate. The overall process of $CaCO_3$ deposition is illustrated in Figure 1, which also reports a sketch of the GIWAXS setup.

Two typologies of experiments were performed, one having the SOM adsorbed on the silicon wafer before $CaCO_3$ deposition (sequential) and one having the SOM in solution mixed with the $CaCO_3$ dispersion (mix). The materials deposited on the silicon wafer, along with the GIWAXS experiments, were characterized by optical microscopy, SEM, EDX mapping, and Raman microscopy. Comparing the results from these two typologies of experiments, we faced some limitations given by the experimental setup used. The amount of material, $CaCO_3$ and SOM, deposited on the substrate can be different. Indeed, in the sequential deposition of SOM and $CaCO_3$, the deposition of $CaCO_3$ mainly occurs during the t_{cast}, as discussed above, whereas a part of the SOM could dissolve in the $CaCO_3$ dispersion. However, we are confident from the experimental observations that this fraction of SOM is very low since SOM has the capability to interact with $CaCO_3$ making precipitates.[33] In the mixing system, the capability of the SOM and the $CaCO_3$ to interact with the substrate can be different, and thus, a different amount of material could be deposited. We considered that the quantification of the final SOM deposited on the substrate using the two different experimental approaches may not represent the material that we are analyzing by GIWAXS due to the inhomogeneity of the precipitate coverage of the substrate evidenced by optical and electron microscopies (see here coming results). However, despite these limitations, which cannot be avoided, the following results are relevant in comparing the behavior of the SOMs from different species in the intra- and inter-experimental setups.

Control and Reference Experiments. A control experiment using only the $CaCO_3$ dispersion and in the absence of SOM was performed. It showed the nonuniform deposition of the material (Figure 2A), which is crystalline, as deduced by the birefringence visible in crossed-polarizers optical images (Figure 2A inset) and arranged in rhombohedral and spherulitic crystals (Figure 2B), the typical morphology of calcite and vaterite phases, respectively. The regions of the substrate among the crystals are not only free of crystalline material, being not birefringent (Figure 2A inset), but also do not contain any $CaCO_3$ materials, as is visible in the EDX spectrum free of signals from calcium and carbon (Figure 2B inset). The presence of the two phases has been confirmed by the analysis of the 2D-GIWAXS images, where the reflections of calcite (marked in white) and vaterite (in red) phases have been indexed. Signals from the underneath Si substrate are marked in black.

The profile of the diffracted intensity integrated over the entire 2D-GIWAXS image (Figure 2A) versus the q vector is reported in Figure S2 (black line). A quantitative analysis (for instance by using the Rietveld method[44]) is not possible due to the diffracted signals coming from polycrystalline materials (vaterite) and single crystals (calcite). However, taking into account that vaterite reflections have scattering factors lower than those of calcite,[45] the diffraction profile (Figure S2) suggests a higher content of vaterite than calcite. This agrees with the distribution of spherical (vaterite) and rhombohedral (calcite) particles observed in the optical and SEM images (Figures S1 and S2). The intensity distribution on the 2D image of the diffraction signals of the two polymorphs provides additional structural information, which highlights the marked

https://doi.org/10.1021/acs.cgd.3c00401
Cryst. Growth Des. 2023, 23, 5801−5811

Table 1. Data Extracted by the Series of 2D-GIWAXS Recorded at Different α_I for Spi SOM, Opa SOM, and $CaCO_3$ Mixed with Spi (Spi_mix) and with Opa (Opa_mix)[a]

	q^1 (Å^{-1})	fwhm^1 (Å^{-})	q^2 (Å^{-1})	fwhm^2 (Å^{-1})	A^1	A^2	$A^2/(A^2 + A^1)$ (%)	$A^s/(A^s + A^b)$ (%)
Spi SOM	0.38	0.08	0.68	0.16	10	33	76	from 5 ($\alpha_{I\,l}$) to 40 ($\alpha_{I\,h}$)
Opa SOM	0.38	0.10	0.67	0.16	9	29	76	from 5 ($\alpha_{I\,l}$) to 40 ($\alpha_{I\,h}$)
Spi SOM mix	0.38	0.08	0.68	0.16	4	9	70	from 0 ($\alpha_{I\,l}$) to 20 ($\alpha_{I\,h}$)
Opa SOM mix	0.34	0.10	0.66	0.18	2	3	60	from 0 ($\alpha_{I\,l}$) to 13 ($\alpha_{I\,h}$)

[a]For the two peaks (see Figure 3) we report the position (q), the width (W), the integrated area (A) and their relative area. From the fit of the azimuthal profiles of peak 2, we determine the two Gaussian contributions [sharp (s) and broad (b), and we report their area ratio from the surface region [lowest α_I ($\alpha_{I\,l}$)] to whole thickness [highest α_I ($\alpha_{I\,h}$)].

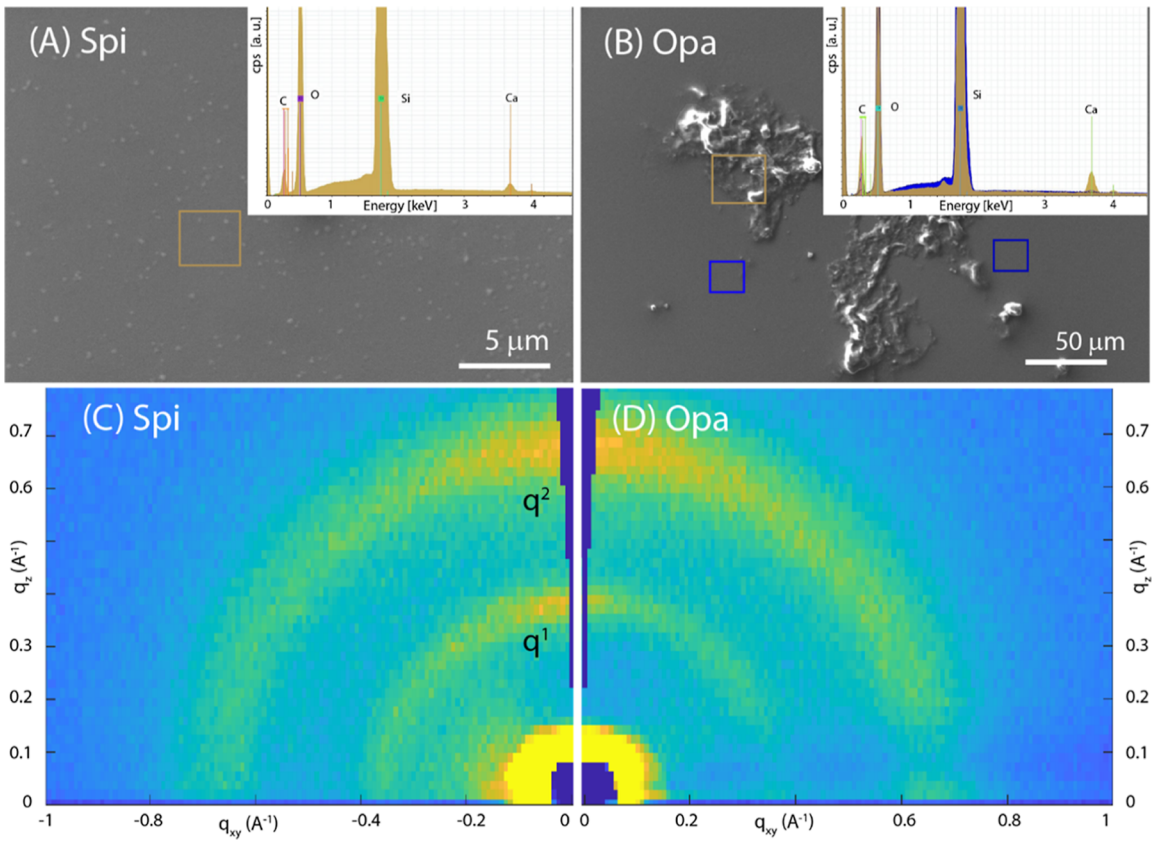

Figure 3. (A,B) SEM images of SOM spin-coated on a silicon wafer from *S. pistillata* (Spi) and *O. patagonica* (Opa), respectively. In the inset the EDX spectra recorded from the square regions drawn on the SEM images are reported. (C,D) 2D-GIWAXS images from Spi and Opa, respectively, deposited on the substrate. q^1 and q^2 indicate the diffraction peaks analyzed in Table 1.

difference in their arrangement on the substrate, in agreement with their different morphologies, as depicted by the SEM image (Figure 2). The intensity distribution of diffracted vaterite reflections indicates the presence of polycrystallites having (001) planes preferentially oriented parallel to the substrate. This suggests that the spherulitic crystals, imaged by SEM, consist of crystallites that may nucleate and grow at the substrate surface, which induces their preferential orientation (Figure S3). This preferential orientation was recently observed in vivo at Lake Sturgeon otolith formation and in synthetic crystals, where vaterite spherulites formed by crystallites.[46] This contrasts with the more common spherulitic growths associated with radiating or concentric textures.[47] On the other hand, the distribution of the spotty diffraction signals of calcite indicates that it forms crystallites having the (104) face mainly parallel to the silicon surface, together with a small fraction of small crystallites almost randomly oriented, which produce weaker almost uniform (ring) signals. From these data, we cannot infer if this crystallite orientation is induced by the substrate presence or by calcite morphology, being the (104) faces the most prominent ones.[48] As additional control experiments, the SOM from each of the two species was spin-coated on the silicon substrate before interaction with the $CaCO_3$ dispersion. The characterization of these substrates is illustrated in Figures 3 and S4−S7.

The SEM images show that the Spi SOM deposits form an almost continuous homogeneous layer on the Si substrate, while the Opa SOM aggregates in some regions of the substrate surface forming rough islands of material. These deposits do not show birefringence (Figures S4A,B and S5A,B), suggesting that there are no birefringent crystalline materials. The EDX spectra (Figure 3 insets) indicated the presence of C as the main element and Ca, as expected, since SOMs were extracted from an aragonitic skeleton. The EDX maps on selected area (Figures S6A,B and S7A,B) confirmed that the two SOMs distribute differently on the substrate

https://doi.org/10.1021/acs.cgd.3c00401
Cryst. Growth Des. 2023, 23, 5801−5811

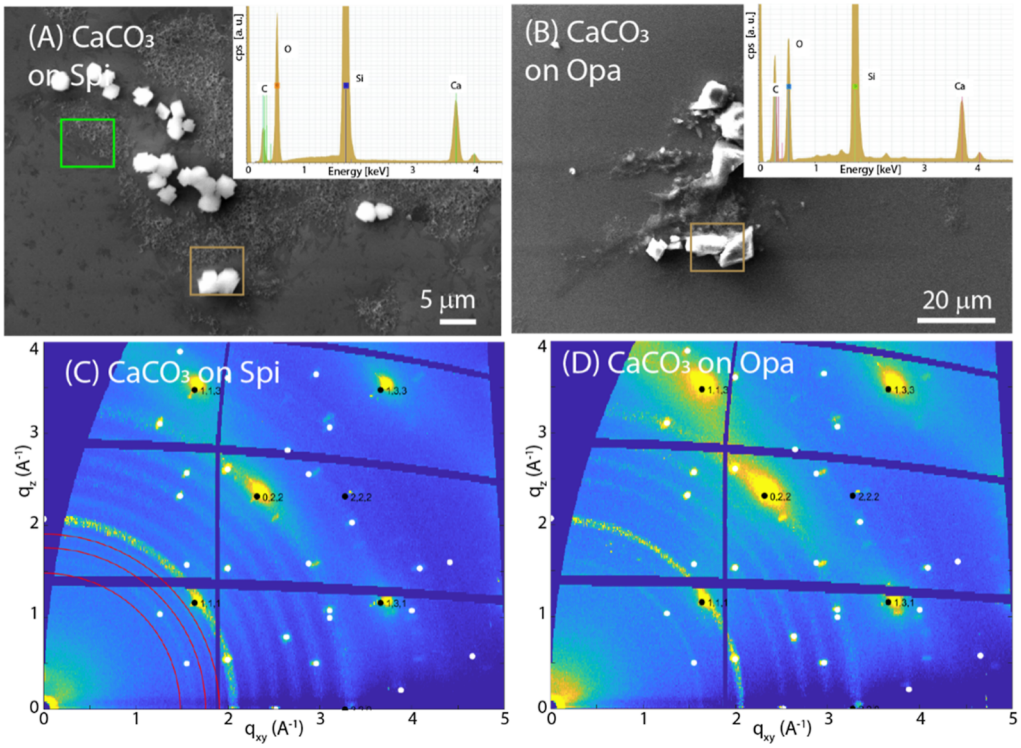

Figure 4. (A,B) SEM images of $CaCO_3$ deposited on the SOM layer from *S. pistillata* or *O. patagonica*, respectively. In the inset, the EDX spectra recorded from the square regions drawn on the SEM images are reported. (C,D) GID images from $CaCO_3$ deposited on the SOM layer from *S. pistillata* or *O. patagonica*, respectively.

surface. Despite these differences, the corresponding 2D-GIWAXS images are extremely similar (Figure 3C,D). Both deposited SOMs produce two diffraction arcs, centered in the vertical direction at the same q_z value, corresponding to the same periodicity. These values could be related to the interactions among the polysaccharidic regions of the SOM glycoproteins and proteoglycans.[49−51]

The literature on the diffraction patterns from SOMs is absent, and in general, for glycoproteins and proteoglycans, it is quite poor. In a diverse context, similar periodicities were observed in crystalline bacterial cell surface layers.[52] As previously observed for cellulose,[53] the presence of two reflections along the out-of-plane direction in GIWAXS images suggests that two populations of crystallites are present, each with a different plane stacked parallel to the surface substrate. One possibility is that these populations are segregated into separate lamella within the sample. Although these reflections could not be indexed, due to the lack of crystallographic data, for the 3D crystalline structure, we expect complementary reflections to be present away from the out-of-plane direction, at an angle that is consistent with the unit cell structure. This is not observed in the GIWAXS data. We hypothesize that the degree of order of chain packing, strong in the out-of-plane direction, is disordered along the plane of the substrate which leads to a diffraction too weak to be detected, suggesting 2D crystal behavior.[54] As different plane surfaces can have diverse hydrophobicity and hydrophilicity, the hydrophobic−hydrophobic and hydrophilic−hydrophilic interactions are likely to be important for intercrystallite interactions.

The analysis of the series of 2D images recorded at different incident angles (see the series for Spi SOM on silicon in Figure S8) allows depth-resolved insights into the SOM arrangement. It is interesting to note that for both SOMs, the two diffraction peaks maintain exactly the same values in q and fwhm, regardless of the incidence angle (see Figure S9 for q and fwhm vs α_i for the second peak of Spi SOM on silicon), i.e., $q^1 = 0.37$ Å $^{-1}$ and $q^2 = 0.68$ Å $^{-1}$, (corresponding to $d = 16.98$ and 9.24 Å, respectively) and fwhm 0.08 and 0.16 Å $^{-1}$, respectively. This indicates that the same crystalline order and dimensions of crystallites are maintained along the film thickness (Table 1).

However, the analysis of the azimuthal profiles indicates a slight depth dependence of molecular misorientation. The experimental azimuthal profile can be reproduced by assuming two Gaussian contributions, a broad and sharp one, associated with crystallites having lower and higher preferential orientation, respectively, i.e., with an associated mosaicity of ∼50 and ∼14°. For both the SOMs, these values are almost constant along the film thickness; however, the relative amount of the two populations changes along the film thickness: the sharp content, estimated by the percentage area ratio, $A = A_{sharp}/(A_{sharp} + A_{broad})\cdot 100$, increases from 5% (close to the air interface) to 40% (close the silicon substrate), indicating a more pronounced stacking alignment close to the substrate surface (Figure S9 for A_p % vs α_i for the second peak of Spi SOM on silicon).

SOM—$CaCO_3$ Sequential Chemical System. The SOM substrates were used for the templated deposition of $CaCO_3$ from the $CaCO_3$ dispersion. The crystallite morphologies and structures, as determined by SEM and GIWAXS data (Figures 2−4 and S4−S7) show that the vaterite is largely suppressed (completely in the case of Opa SOM) and mainly the calcite phase forms on the two SOMs deposited substrates, differently from the control in which vaterite was the dominant phase. This result is apparently in contradiction with recent experiments that showed the stabilization of vaterite from

https://doi.org/10.1021/acs.cgd.3c00401
Cryst. Growth Des. 2023, 23, 5801−5811

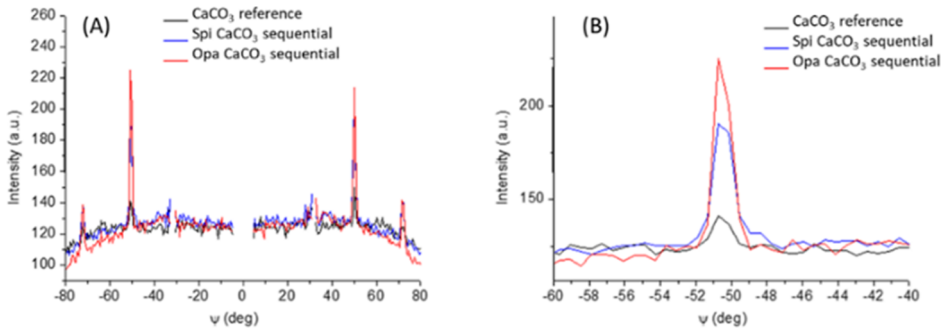

Figure 5. (A) Azimuthal profiles of the (10−2) reflection of calcite extracted from 2D-GIWAXS images of the reference $CaCO_3$ sample (black curve from Figure 2E), and sequentially deposited $CaCO_3$ on Spi SOM (blue curve from Figure 4C) and on Opa SOM (red curve from Figure 4D) samples. (B) Zoom of one azimuthal peak reported in (A).

SOM macromolecules from the coral skeleton.[33,55] However, it has to be considered that in one case the vaterite formation was observed using a specific protein of the SOM, the CARP3, in the presence of magnesium ions in solution.[55] In another case, the vaterite formed on magnesium calcite seeds in the presence of SOM from *S. pistillata*, hence involving the presence of magnesium ions.[33] In the absence of magnesium ions, it has been reported for a long time that several polyelectrolytes inhibit the formation of vaterite.[56] SOMs in their protein components are rich in charged Asp and Glu and therefore can inhibit the vaterite formation.[32]

The SEM images (Figure 4A,B) indicate that the calcite formation occurs preferentially in the regions where the SOM substrate was present: crystallites are not detected on a smooth surface, associated with the neat silicon wafer, and the EDX mapping does not show the presence of calcium (Figures S6 and S7). Interestingly, the SOMs after the interaction with the $CaCO_3$ dispersion (i) lost their layered crystalline structure and (ii) reorganized their distribution of the surfaces. The former is deduced by the lack of low angle diffraction signals in GIWAXS images (Figure S10) and the latter by the OM and SEM images (Figures 4, S6, and S7). This observation suggests that the SOM substrates are not rigid structures, but upon interaction with the $CaCO_3$ particles dispersion, they lose the periodic order, partially dissolve, and reaggregate. On the GIWAXS images (Figure 4C,D) the diffraction signals of vaterite reflections are weaker (in the case of Spi SOM) than the corresponding reference samples or completely absent (in the case of Opa SOM), whereas the calcite diffraction spots are not affected by the presence of the SOM. These results indicate that the vaterite phase, dominant in the reference system, is largely suppressed by the presence of the SOM. From these data, it seems that the SOM molecules do not lose the capability to interact with $CaCO_3$ particles favoring their crystallization and eventually orientation. Indeed, 2D-GIWAXS data indicate the same arrangement observed for the reference samples, but the SOM presence induces an increase in the ratio of single crystals to polycrystals, as deduced by the increased intensity of the spots compared to the broad contribution, as clearly seen in the azimuthal profiles (Figure 5A,B).

Additional information was obtained from the Raman spectroscopy images (Figure 6). Calcite was colored according to the Eg vibration at about 280 cm^{-1}, ACC was colored according to the broad vibration at 1080 cm^{-1}, and Si was recognized by the phonon at 520.7 cm^{-1}. It is easier than trying to differentiate between the two peaks at around 1086 cm^{-1} narrow for calcite and broad for ACC centered around

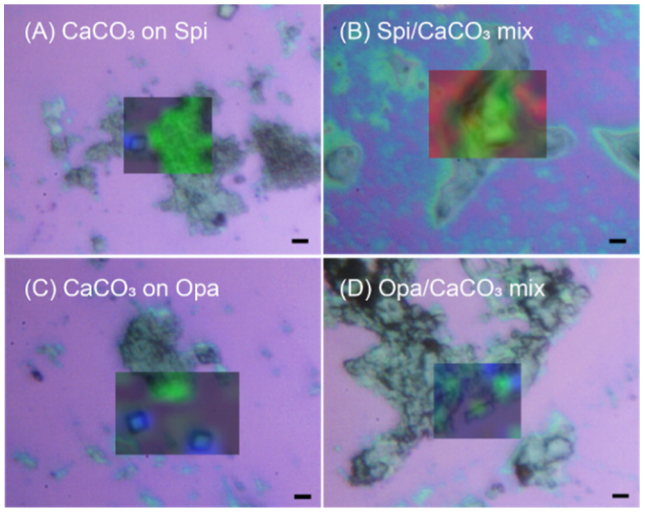

Figure 6. Micro-Raman microscopy analyses on $CaCO_3$ deposited on silicon substrates by sequential or mixing experiments showing optical microscopy images and $CaCO_3$ phase overlaid color Raman maps. (A,B) $CaCO_3$ deposited on the Spi SOM substrate from a $CaCO_3$ dispersion (A) and on the silicon substrate from a Spi SOM−$CaCO_3$ mixture (B). (C,D) $CaCO_3$ deposited on the Opa SOM substrate from a $CaCO_3$ dispersion (C) and on the silicon substrate from an Opa SOM−$CaCO_3$ mixture (D). In the overlaid color Raman map, green indicates ACC and blue indicates calcite. The red background is due to the silicon substrate. The mineral phases were assigned according with previous studies.[33,34] Scale bar: 4 μm.

1080 cm^{-1}. The Raman spectra confirmed the presence of calcite in the samples and also showed the copresence of ACC (Figure 6A,C). The latter was observed in the nonbirefringent aggregates and appeared in association with the SOM matrices. The Raman data did not show relevant differences between the SOM from *S. pistillata* and that from *O. patagonica*. The presence of ACC indicates not only that the crystalline phase formed from ACC,[39] as expected from the starting condition of supersaturation, but also that the SOM from both species interacts and stabilizes the ACC[40] since in the control experiments, only crystalline phases were observed (Figure 2). The Raman spectra as well as GIWAX images were collected on dry samples obtained by spin coating. We hypothesize that these dry samples are chemically stable. The observation of ACC indicates that it is in a stable form, able to remain unchanged for a period of months.

In general, the results from this first set of experiments generally agree with what was observed by the Addadi group in

https://doi.org/10.1021/acs.cgd.3c00401
Cryst. Growth Des. 2023, 23, 5801−5811

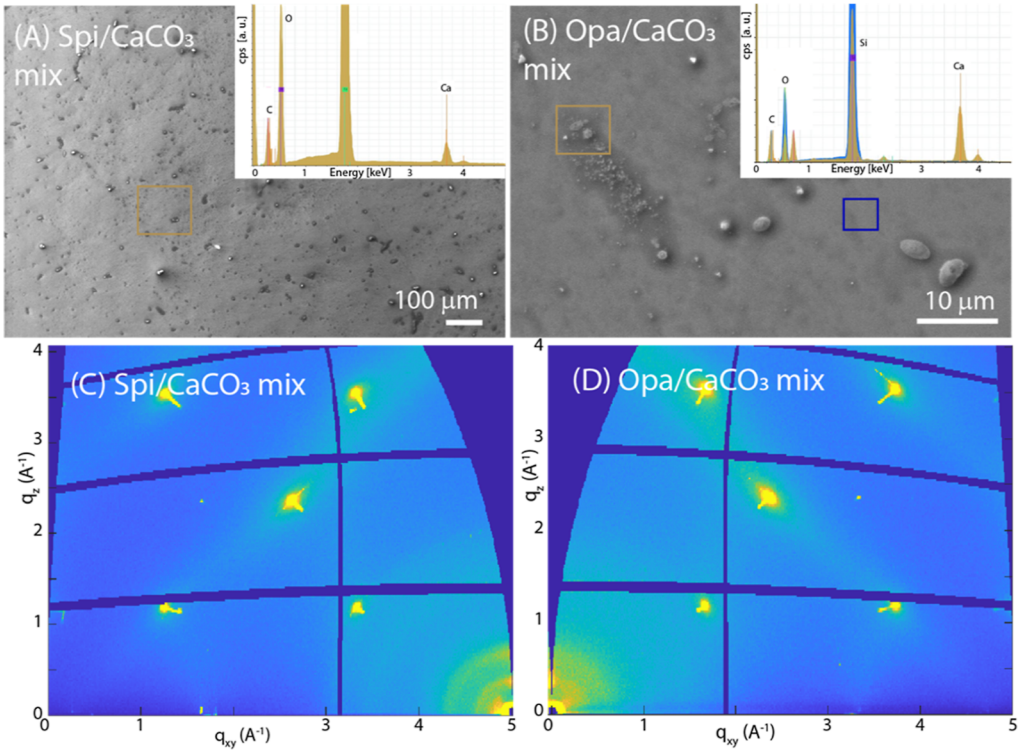

Figure 7. (A,B) SEM images of a $CaCO_3$/SOM mix deposited on a silica substrate with SOM from *S. pistillata* or *O. patagonica*, respectively. In the inset, the EDX spectra recorded from the square regions drawn on the SEM images are reported. (C,D) GID images from $CaCO_3$/SOM mix deposited on silica substrate with SOM from *S. pistillata* or *O. patagonica*, respectively.

a pioneering work using SOM from mollusk shells.[23] In those studies, a preferential [001] orientation of calcite crystals was observed on a glass substrate where SOM was adsorbed before the crystallization of calcite by the ammonium carbonate vapor diffusion method.[23] Here, we add the information that the formation of the calcite crystals occurs through an ACC phase that is stabilized by the SOM. Thus, the SOM, when adsorbed on a substrate, stabilizes the ACC phase and influences the orientation of the crystals.

SOM–$CaCO_3$ Mix Chemical System. The formation of crystalline faces was not observed when the SOMs were mixed with the $CaCO_3$ dispersion before $CaCO_3$ deposition on the silicon substrate. Also, the polarization optical microscopy images did not show any birefringence (Figures S4 and S5) and no mineral $CaCO_3$ diffraction effect was present in the GIWAXS images (Figure 7), but the EDX mapping showed a strong signal for Ca and C (Figures S6 and S7). In these samples, the Raman microscopy mapping (Figure 6B,D) showed a clear signal from ACC.[57] It is possible that as the SOM can stabilize ACC,[3] it represents an aspect of the inhibition of crystallization. In addition to this observation, in the presented case, it seems that the presence of ACC does not affect the SOM arrangement in the case of the Spi SOM, whose peak diffraction positions, i.e., periodicities, widths, and the mosaicity attain to the values of the film obtained without $CaCO_3$ present (Figure S11, Table 1). The Opa SOM molecules still self-assemble on the silicon substrate but in a less efficient way, as witnessed by the extremely low scattered signal, which is almost absent for the second peak (Figure S11B). The first peak has a larger periodicity than that determined for the reference sample, indicating a structural change (Table 1).

General Considerations. The above results, once more, indicate that much of the knowledge on SOM from mollusk shells also applies to coral skeletons, even if the latter does not present a high level of control on the mineral texture. An observation that agrees with a general calcification strategy reported in a recent paper.[58] However, this study sheds new light on the pioneering research of Weiner and Hood,[59] and Wheeler et al.[60] also addressing aspects related to crystallography. We show that SOM macromolecules play diverse roles depending on their assembly/aggregation state. When they are adsorbed onto a template and have an initial structure,[21,22] they can promote crystal nucleation through the ACC transient phase, but when in solution, they inhibit crystal growth stabilizing the ACC. The initial nucleation model of Weiner et al.,[22] which was developed from mollusk shell biomineralization, was based on proteins adopting an ordered conformation (the antiparallel β-sheet) and adsorbed on the faces of a substrate (the chitin core). In this "sandwich" model, the carboxylate groups of the side chains of proteins and sulfated polysaccharides contributed to set the conditions for mineral deposition in a heteroepitaxy model.[23] Later, it was shown that in nacre samples, a gelling state occurs in the organo-mineral assembly,[61,62] and that the tablet is surrounded by a thin layer of ACC.[63] The most recent model of $CaCO_3$ biomineralization suggests that the mineral deposition occurs by particle attachments of ACC on the mineral surface,[14] that is present in a gelling environment. On the contrary, in corals' SOM, no evidence of β-sheet order confirmation was reported, but most SOM identified to have at least one intrinsic disorder region providing a building block for mineral deposition.[32] Our data suggest that the SOM has a layered structure and that this structural organization is lost when the oriented mineral deposition occurs. However, this layered organization is still

https://doi.org/10.1021/acs.cgd.3c00401
Cryst. Growth Des. 2023, 23, 5801−5811

present when ACC is dispersed into the SOM. We are not able to assess whether the initial formation of ACC occurs on SOM absorbed on the substrate, but we observe that the crystalline layered assembly of SOM is lost when calcite crystals are formed. This layered state is instead conserved when SOM is mixed in $CaCO_3$ particles dispersion. We are confident that this layered structure could also be generated by SOM extracted by other species of corals. Indeed, in our previous research it was observed that the chemical composition of the SOM is quite similar among species, being characterized by a high content of aspartic and glutamic residues and being the proteins glycosylated.[3,32,35,64]

Based on our experimental results, we propose the following model: SOM adsorbed on the substrate initially interacts with the ACC particles and preserves its layered structure; when the crystallization process occurs, the macromolecules of SOM may influence the orientation of the calcite crystals but lose their stratified structure. We can suppose that, being the SOM proteins intrinsically disordered,[32] the control of crystal orientation, if not governed by the morphology of calcite, could be attributed to geometrical restrains,[65] differently from what reported for mollusk, where proteins assume a beta structure.[23] What triggers the transition from the amorphous to the crystalline phase is not determinable in this study. It is also important to consider the formation of calcite instead of aragonite, the mineral phase forming the coral skeleton, as expected since in in vitro experiments aragonite forms at room temperature only in the presence of Mg ions.[66] The use of Mg ions was avoided to reduce the complexity of the system and considering that the used chemical system is a model for the study of the biomineralization process.[67]

However, on the basis of the presented results, it can be assumed that in the in vivo system, the different macromolecules that make up SOM can be secreted by the cells at different times and spaces, carrying out their activities in the right space and time. This model is in good agreement with the two-step mode of growth proposed by Cuif and co-workers for the biomineralization of corals,[31,68] which supposes an initial formation of a macromolecular layer on which the oriented deposition of aragonite crystals takes place.

CONCLUSIONS

In this study, we showed that SOM from coral skeleton can assemble in an ordered layered structure and that it can induce the oriented crystallization of calcite. Furthermore, we demonstrated that the layered structure remains even when trapped ACC is present but is lost when ACC crystallizes. This observation is completely new for coral and integrates and enriches the biomineralization model for mollusks proposed by Addadi and Weiner,[2,69] and Weiner and Traub.[20,22] We are confident that this approach to the study of coral biomineralization processes will contribute to a significant improvement in the understanding of biomineralization processes, inspiring studies on different substrates and with different SOMs. It will also awaken the interest of researchers in the study of the crystallographic aspects of biomineralization, which still represents one of the most intriguing aspects of biominerals.

ASSOCIATED CONTENT

Supporting Information

The Supporting Information is available free of charge at https://pubs.acs.org/doi/10.1021/acs.cgd.3c00401.

Detailed description of the optimization of the experimental setup, optical microscopy images, sample EDX maps, and additional 2D-GIWAXS data (PDF)

AUTHOR INFORMATION

Corresponding Authors

Silvia Milita − *CNR—Institute for Microelectronic and Microsystems, Bologna 40129, Italy;* orcid.org/0000-0002-9612-2541; Email: milita@bo.imm.cnr.it

Giuseppe Falini − *Department of Chemistry "Giacomo Ciamician", University of Bologna, Bologna 40126, Italy; CNR, Institute for Nanostructured Materials, Bologna 40129, Italy;* orcid.org/0000-0002-2367-3721; Email: giuseppe.falini@unibo.it

Tali Mass − *Department of Marine Biology, The Leon H. Charney School of Marine Sciences, University of Haifa, Haifa 3498838, Israel*; Email: tmass@univ.haifa.ac.il

Authors

Tal Zaquin − *Department of Marine Biology, The Leon H. Charney School of Marine Sciences, University of Haifa, Haifa 3498838, Israel*

Simona Fermani − *Department of Chemistry "Giacomo Ciamician", University of Bologna, Bologna 40126, Italy; Interdepartmental Centre for Industrial Research Health Sciences & Technologie, University of Bologna, Bologna 40064, Italy*

Devis Montroni − *Department of Chemistry "Giacomo Ciamician", University of Bologna, Bologna 40126, Italy*

Iddo Pinkas − *Department of Chemical Research Support, Weizmann Institute of Science, Rehovot 76100, Israel;* orcid.org/0000-0001-7434-9844

Luisa Barba − *CNR -Institute of Crystallography, Elettra Synchrotron, Trieste I-34100, Italy*

Complete contact information is available at: https://pubs.acs.org/10.1021/acs.cgd.3c00401

Author Contributions

The manuscript was written through contributions of all authors. All authors have given approval to the final version of the manuscript.

Funding

This project was also funded by the European Research Council (ERC) under the European Union's Horizon 2020 research and innovation program (grant agreement no. 755876 to T.M.).

Notes

The authors declare no competing financial interest.

ACKNOWLEDGMENTS

We wish to thank the Synchrotron Radiation Source Electra (Trieste, Italy) and the XRD1 beamline staff (Elettra) for the support provided during the measurements. We thank Dr. Damir Kralj (Ruder Boskovic Institute, Croatia) for the help in the study of calcium carbonate chemistry. We thank the Institute for Microelectronic and Microsystems (CNR, Italy) and Dr. Franco Corticelli for the support in the electron microscopy analyses. I.P. is the incumbent of the Sharon Zuckerman research fellow chair.

REFERENCES

(1) Lowenstam, H. A.; Weiner, S. *On Biomineralization*; Oxford University Press on Demand, 1989.
(2) Addadi, L.; Weiner, S. Biomineralization: Mineral Formation by Organisms. *Phys. Scr.* **2014**, *89*, 098003.
(3) Falini, G.; Fermani, S.; Goffredo, S. Coral Biomineralization: A Focus on Intra-Skeletal Organic Matrix and Calcification. In *Seminars in cell & developmental biology*; Elsevier, 2015; Vol. *46*, pp 17−26.
(4) Drake, J. L.; Mass, T.; Stolarski, J.; Von Euw, S.; Schootbrugge, B.; Falkowski, P. G. How Corals Made Rocks through the Ages. *Global Change Biol.* **2020**, *26* (1), 31−53.
(5) Stolarski, J.; Coronado, I.; Murphy, J. G.; Kitahara, M. V.; Janiszewska, K.; Mazur, M.; Gothmann, A. M.; Bouvier, A.-S.; Marin-Carbonne, J.; Taylor, M. L.; et al. A Modern Scleractinian Coral with a Two-Component Calcite−Aragonite Skeleton. *Proc. Natl. Acad. Sci. U.S.A.* **2021**, *118* (3), 118.
(6) Falini, G.; Albeck, S.; Weiner, S.; Addadi, L. Control of Aragonite or Calcite Polymorphism by Mollusk Shell Macromolecules. *Science* **1996**, *271*, 67−69.
(7) Zolotoyabko, E.; Pokroy, B. Biomineralization of Calcium Carbonate: Structural Aspects. *CrystEngComm* **2007**, *9*, 1156−1161.
(8) Erez, J. The Source of Ions for Biomineralization in Foraminifera and Their Implications for Paleoceanographic Proxies. *Rev. Mineral. Geochem.* **2003**, *54* (1), 115−149.
(9) Bianco-Stein, N.; Polishchuk, I.; Seiden, G.; Villanova, J.; Rack, A.; Zaslansky, P.; Pokroy, B. Helical Microstructures of the Mineralized Coralline Red Algae Determine Their Mechanical Properties. *Adv. Sci.* **2020**, *7* (11), 2000108.
(10) Killian, C. E.; Wilt, F. H. Molecular Aspects of Biomineralization of the Echinoderm Endoskeleton. *Chem. Rev.* **2008**, *108* (11), 4463−4474.
(11) Wang, R. Z.; Addadi, L.; Weiner, S. Design Strategies of Sea Urchin Teeth: Structure, Composition and Micromechanical Relations to Function. *Philos. Trans. R. Soc. London, Ser. B* **1997**, *352* (1352), 469−480.
(12) Weiss, I. M.; Tuross, N.; Addadi, L. I. A.; Weiner, S. Mollusc Larval Shell Formation: Amorphous Calcium Carbonate Is a Precursor Phase for Aragonite. *J. Exp. Zool.* **2002**, *293* (5), 478−491.
(13) Gal, A.; Habraken, W.; Gur, D.; Fratzl, P.; Weiner, S.; Addadi, L. Calcite Crystal Growth by a Solid-state Transformation of Stabilized Amorphous Calcium Carbonate Nanospheres in a Hydrogel. *Angew. Chem., Int. Ed.* **2013**, *52* (18), 4867−4870.
(14) Gilbert, P. U. P. A.; Bergmann, K. D.; Boekelheide, N.; Tambutté, S.; Mass, T.; Marin, F.; Adkins, J. F.; Erez, J.; Gilbert, B.; Knutson, V.; et al. Biomineralization: Integrating Mechanism and Evolutionary History. *Sci. Adv.* **2022**, *8* (10), No. eabl9653.
(15) Okhrimenko, D. V.; Nissenbaum, J.; Andersson, M. P.; Olsson, M. H. M.; Stipp, S. L. S. Energies of the Adsorption of Functional Groups to Calcium Carbonate Polymorphs: The Importance of -OH and -COOH Groups. *Langmuir* **2013**, *29* (35), 11062−11073.
(16) Innocenti Malini, R.; Finney, A. R.; Hall, S. A.; Freeman, C. L.; Harding, J. H. The Water−Amorphous Calcium Carbonate Interface and Its Interactions with Amino Acids. *Cryst. Growth Des.* **2017**, *17* (11), 5811−5822.
(17) Von Euw, S.; Azaïs, T.; Manichev, V.; Laurent, G.; Pehau-Arnaudet, G.; Rivers, M.; Murali, N.; Kelly, D. J.; Falkowski, P. G. Solid-State Phase Transformation and Self-Assembly of Amorphous Nanoparticles into Higher-Order Mineral Structures. *J. Am. Chem. Soc.* **2020**, *142* (29), 12811−12825.
(18) Gómez-Morales, J.; Falini, G.; García-Ruiz, J. M. Biological Crystallization. In *Handbook of crystal growth*; Elsevier, 2015, pp 873−913.
(19) Mann, S. Molecular Recognition in Biomineralization. *Nature* **1988**, *332* (6160), 119−124.
(20) Weiner, S.; Traub, W. X-ray Diffraction Study of the Insoluble Organic Matrix of Mollusk Shells. *FEBS Lett.* **1980**, *111* (2), 311−316.
(21) Weiner, S.; Talmon, Y.; Traub, W. Electron Diffraction of Mollusc Shell Organic Matrices and Their Relationship to the Mineral Phase. *Int. J. Biol. Macromol.* **1983**, *5*, 325−328.
(22) Weiner, S.; Traub, W.; Miller, A.; Phillips, D. C.; Williams, R. J. P. Macromolecules in Mollusc Shells and Their Functions in Biomineralization. *Philos. Trans. R. Soc. London, Ser. B* **1984**, *304* (1121), 425−434.
(23) Addadi, L.; Moradian, J.; Shay, E.; Maroudas, N. G.; Weiner, S. A Chemical Model for the Cooperation of Sulfates and Carboxylates in Calcite Crystal Nucleation: Relevance to Biomineralization. *Proc. Natl. Acad. Sci. U.S.A.* **1987**, *84* (9), 2732−2736.
(24) Stoev, K. N.; Sakurai, K. Review on Grazing Incidence X-Ray Spectrometry and Reflectometry. *Spectrochim. Acta, Part B* **1999**, *54* (1), 41−82.
(25) Kewalramani, S.; Kim, K.; Stripe, B.; Evmenenko, G.; Dommett, G. H. B.; Dutta, P. Observation of an Organic−Inorganic Lattice Match during Biomimetic Growth of (001)-Oriented Calcite Crystals under Floating Sulfate Monolayers. *Langmuir* **2008**, *24* (19), 10579−10582.
(26) Li, Q.; Fernandez-Martinez, A.; Lee, B.; Waychunas, G. A.; Jun, Y.-S. Interfacial Energies for Heterogeneous Nucleation of Calcium Carbonate on Mica and Quartz. *Environ. Sci. Technol.* **2014**, *48* (10), 5745−5753.
(27) Anne, S.; Rozenbaum, O.; Andreazza, P.; Rouet, J.-L. Evidence of a bacterial carbonate coating on plaster samples subjected to the Calcite Bioconcept biomineralization technique. *Constr. Build. Mater.* **2010**, *24*, 1036−1042.
(28) DiMasi, E.; Kwak, S.-Y.; Amos, F. F.; Olszta, M. J.; Lush, D.; Gower, L. B. Complementary Control by Additives of the Kinetics of Amorphous CaCO 3 mineralization at an Organic Interface: In-Situ Synchrotron X-Ray Observations. *Phys. Rev. Lett.* **2006**, *97* (4), 045503.
(29) DiMasi, E.; Kwak, S.-Y.; Pichon, B. P.; Sommerdijk, N. A. J. M. Structural Adaptability in an Organic Template for CaCO 3 mineralization. *CrystEngComm* **2007**, *9* (12), 1192−1204.
(30) Allemand, D.; Tambutté, É.; Zoccola, D.; Tambutté, S. Coral Calcification, Cells to Reefs. *Coral Reefs: An Ecosystem in Transition*, 2011; pp 119−150..
(31) Cuif, J.-P.; Dauphin, Y. The Two-Step Mode of Growth in the Scleractinian Coral Skeletons from the Micrometre to the Overall Scale. *J. Struct. Biol.* **2005**, *150* (3), 319−331.
(32) Zaquin, T.; Di Bisceglie, A. P.; Pinkas, I.; Falini, G.; Mass, T. Different Skeletal Protein Toolkits Achieve Similar Structure and Performance in the Tropical Coral Stylophora Pistillata and the Temperate Oculina Patagonica. *Sci. Rep.* **2022**, *12* (1), 16575.
(33) Zaquin, T.; Pinkas, I.; Di Bisceglie, A. P.; Mucaria, A.; Milita, S.; Fermani, S.; Goffredo, S.; Mass, T.; Falini, G. Exploring Coral Calcification by Calcium Carbonate Overgrowth Experiments. *Cryst. Growth Des.* **2022**, *22* (8), 5045−5053.
(34) Akiva, A.; Neder, M.; Kahil, K.; Gavriel, R.; Pinkas, I.; Goobes, G.; Mass, T. Minerals in the Pre-Settled Coral Stylophora Pistillata Crystallize via Protein and Ion Changes. *Nat. Commun.* **2018**, *9* (1), 1880.
(35) Reggi, M.; Fermani, S.; Landi, V.; Sparla, F.; Caroselli, E.; Gizzi, F.; Dubinsky, Z.; Levy, O.; Cuif, J.-P.; Dauphin, Y.; et al. Biomineralization in Mediterranean Corals: The Role of the Intraskeletal Organic Matrix. *Cryst. Growth Des.* **2014**, *14* (9), 4310−4320.
(36) Kralj, D.; Kontrec, J.; Brečević, L.; Falini, G.; Nöthig-Laslo, V. Effect of Inorganic Anions on the Morphology and Structure of Magnesium Calcite. *Chem.—Eur. J.* **2004**, *10* (7), 1647−1656.
(37) Štajner, L.; Kontrec, J.; Njegić Džakula, B.; Maltar-Strmečki, N.; Plodinec, M.; Lyons, D. M.; Kralj, D. The Effect of Different Amino Acids on Spontaneous Precipitation of Calcium Carbonate Polymorphs. *J. Cryst. Growth* **2018**, *486*, 71−81.
(38) Njegic-Dzakula, B.; Brecevic, L.; Falini, G.; Kralj, D. Calcite Crystal Growth Kinetics in the Presence of Charged Synthetic Polypeptides. *Cryst. Growth Des.* **2009**, *9* (5), 2425−2434.

https://doi.org/10.1021/acs.cgd.3c00401
Cryst. Growth Des. 2023, 23, 5801−5811

(39) Njegić-Džakula, B.; Falini, G.; Brečević, L.; Skoko, Ž.; Kralj, D. Effects of Initial Supersaturation on Spontaneous Precipitation of Calcium Carbonate in the Presence of Charged Poly-l-Amino Acids. *J. Colloid Interface Sci.* **2010**, *343* (2), 553−563.
(40) Mass, T.; Giuffre, A. J.; Sun, C.-Y.; Stifler, C. A.; Frazier, M. J.; Neder, M.; Tamura, N.; Stan, C. V.; Marcus, M. A.; Gilbert, P. U. P. A. Amorphous Calcium Carbonate Particles Form Coral Skeletons. *Proc. Natl. Acad. Sci. U.S.A.* **2017**, *114* (37), E7670−E7678.
(41) Kralj, D.; Brečević, L.; Nielsen, A. E. Vaterite Growth and Dissolution in Aqueous Solution I. Kinetics of Crystal Growth. *J. Cryst. Growth* **1990**, *104* (4), 793−800.
(42) Gebauer, D.; Kellermeier, M.; Gale, J. D.; Bergström, L.; Cölfen, H. Pre-Nucleation Clusters as Solute Precursors in Crystallisation. *Chem. Soc. Rev.* **2014**, *43* (7), 2348−2371.
(43) Sarkar, A.; Mahapatra, S. Synthesis of All Crystalline Phases of Anhydrous Calcium Carbonate. *Cryst. Growth Des.* **2010**, *10* (5), 2129−2135.
(44) Doebelin, N.; Kleeberg, R. Profex: A Graphical User Interface for the Rietveld Refinement Program BGMN. *J. Appl. Crystallogr.* **2015**, *48* (5), 1573−1580.
(45) Rez, D.; Rez, P.; Grant, I. Dirac−Fock Calculations of X-Ray Scattering Factors and Contributions to the Mean Inner Potential for Electron Scattering. *Acta Crystallogr., Sect. A: Found. Crystallogr.* **1994**, *50* (4), 481−497.
(46) Chakoumakos, B. C.; Pracheil, B. M.; Wood, R. S.; Loeppky, A.; Anderson, G.; Koenigs, R.; Bruch, R. Texture Analysis of Polycrystalline Vaterite Spherulites from Lake Sturgeon Otoliths. *Sci. Rep.* **2019**, *9* (1), 7151.
(47) Wang, J.; Becker, U. Structure and Carbonate Orientation of Vaterite (CaCO3). *Am. Mineral.* **2009**, *94* (2−3), 380−386.
(48) Gonzalez, L. A.; Carpenter, S. J.; Lohmann, K. C. Inorganic Calcite Morphology; Roles of Fluid Chemistry and Fluid Flow. *J. Sediment. Res.* **1992**, *62* (3), 382−399.
(49) Tambutté, S.; Tambutté, E.; Zoccola, D.; Allemand, D. Organic Matrix and Biomineralization of Scleractinian Corals. *Handbook of Biomineralization: Biological Aspects and Structure Formation*, 2007; pp 243−259..
(50) Marin, F.; Luquet, G. Unusually Acidic Proteins in Biomineralization. *Handbook of Biomineralization: Biological Aspects and Structure Formation*, 2007; pp 273−290..
(51) Arias, J. L.; Fernández, M. S. Polysaccharides and Proteoglycans in Calcium Carbonate-Based Biomineralization. *Chem. Rev.* **2008**, *108* (11), 4475−4482.
(52) Sleytr, U. B.; Messner, P.; Pum, D.; Sára, M. Crystalline Bacterial Cell Surface Layers (S Layers): From Supramolecular Cell Structure to Biomimetics and Nanotechnology. *Angew. Chem., Int. Ed.* **1999**, *38* (8), 1034−1054.
(53) Ye, D.; Rongpipi, S.; Kiemle, S. N.; Barnes, W. J.; Chaves, A. M.; Zhu, C.; Norman, V. A.; Liebman-Peláez, A.; Hexemer, A.; Toney, M. F.; et al. Preferred Crystallographic Orientation of Cellulose in Plant Primary Cell Walls. *Nat. Commun.* **2020**, *11* (1), 4720.
(54) Bodík, M.; Krajčíková, D.; Hagara, J.; Majkova, E.; Barák, I.; Šiffalovič, P. Diffraction Pattern of Bacillus Subtilis CotY Spore Coat Protein 2D Crystals. *Colloids Surf., B* **2021**, *197*, 111425.
(55) Laipnik, R.; Bissi, V.; Sun, C.-Y.; Falini, G.; Gilbert, P. U. P. A.; Mass, T. Coral Acid Rich Protein Selects Vaterite Polymorph in Vitro. *J. Struct. Biol.* **2020**, *209* (2), 107431.
(56) Falini, G.; Gazzano, M.; Ripamonti, A. Crystallization of Calcium Carbonate in Presence of Magnesium and Polyelectrolytes. *J. Cryst. Growth* **1994**, *137* (3−4), 577−584.
(57) Wang, D.; Hamm, L. M.; Bodnar, R. J.; Dove, P. M. Raman Spectroscopic Characterization of the Magnesium Content in Amorphous Calcium Carbonates. *J. Raman Spectrosc.* **2012**, *43* (4), 543−548.
(58) Gilbert, P. U. P. A.; Porter, S. M.; Sun, C.-Y.; Xiao, S.; Gibson, B. M.; Shenkar, N.; Knoll, A. H. Biomineralization by Particle Attachment in Early Animals. *Proc. Natl. Acad. Sci. U.S.A.* **2019**, *116* (36), 17659−17665.
(59) Weiner, S.; Hood, L. Soluble Protein of the Organic Matrix of Mollusk Shells: A Potential Template for Shell Formation. *Science* **1975**, *190* (4218), 987−989.
(60) Wheeler, A. P.; George, J. W.; Evans, C. A. Control of Calcium Carbonate Nucleation and Crystal Growth by Soluble Matrx of Oyster Shell. *Science* **1981**, *212* (4501), 1397−1398.
(61) Levi-Kalisman, Y.; Falini, G.; Addadi, L.; Weiner, S. Structure of the Nacreous Organic Matrix of a Bivalve Mollusk Shell Examined in the Hydrated State Using Cryo-TEM. *J. Struct. Biol.* **2001**, *135*, 8−17.
(62) Addadi, L.; Joester, D.; Nudelman, F.; Weiner, S. Mollusk Shell Formation: A Source of New Concepts for Understanding Biomineralization Processes. *Chemistry* **2006**, *12* (4), 980−987.
(63) Nassif, N.; Pinna, N.; Gehrke, N.; Antonietti, M.; Jäger, C.; Cölfen, H. Amorphous Layer around Aragonite Platelets in Nacre. *Proc. Natl. Acad. Sci. U.S.A.* **2005**, *102* (36), 12653−12655.
(64) Falini, G.; Reggi, M.; Fermani, S.; Sparla, F.; Goffredo, S.; Dubinsky, Z.; Levi, O.; Dauphin, Y.; Cuif, J. P. Control of Aragonite Deposition in Colonial Corals by Intra-Skeletal Macromolecules. *J. Struct. Biol.* **2013**, *183*, 226−238.
(65) Checa, A. G.; Rodríguez-Navarro, A. Geometrical and Crystallographic Constraints Determine the Self-Organization of Shell Microstructures in Unionidae (Bivalvia: Mollusca). *Proc. R. Soc. London, Ser. B* **2001**, *268* (1468), 771−778.
(66) Goffredo, S.; Vergni, P.; Reggi, M.; Caroselli, E.; Sparla, F.; Levy, O.; Dubinsky, Z.; Falini, G. The Skeletal Organic Matrix from Mediterranean Coral Balanophyllia Europaea Influences Calcium Carbonate Precipitation. *PLoS One* **2011**, *6* (7), No. e22338.
(67) Albeck, S.; Weiner, S.; Addadi, L. Polysaccharides of Intracrystalline Glycoproteins Modulate Calcite Crystal Growth in Vitro. *Chem.—Eur. J.* **1996**, *2* (3), 278−284.
(68) Baronnet, A.; Cuif, J.-P.; Dauphin, Y.; Farre, B.; Nouet, J. Crystallization of Biogenic Ca-Carbonate within Organo-Mineral Micro-Domains. Structure of the Calcite Prisms of the Pelecypod Pinctada Margaritifera (Mollusca) at the Submicron to Nanometre Ranges. *Mineral. Mag.* **2008**, *72* (2), 617−626.
(69) Albeck, S.; Aizenberg, J.; Addadi, L.; Weiner, S. Interactions of Various Skeletal Intracrystalline Components with Calcite Crystals. *J. Am. Chem. Soc.* **1993**, *115* (25), 11691−11697.

https://doi.org/10.1021/acs.cgd.3c00401
Cryst. Growth Des. 2023, 23, 5801−5811